Biophysical Journal
Article

Biophysical Society

Mechanism of Nucleotidyltransfer Reaction and Role of Mg^{2+} Ion in Sugar Nucleotidyltransferases

Neha Vithani,[1] Balaji Prakash,[2,*] and Nisanth N. Nair[3,*]
[1]Department of Biological Sciences and Bioengineering, Indian Institute of Technology, Kanpur, India; [2]Department of Molecular Nutrition, CSIR-Central Food Technological Research Institute, Mysore, India; and [3]Department of Chemistry, Indian Institute of Technology, Kanpur, India

ABSTRACT Sugar nucleotidyl transferases (SNTs) catalyze nucleotidyltransfer reactions to form sugar-nucleotides and pyrophosphate in the presence of two Mg^{2+} ions (Mg^{2+}_A and Mg^{2+}_B). We unveil the mechanism and free energetics of nucleotidyl transfer reaction in an SNT called GlmU through hybrid quantum mechanics-molecular mechanics molecular dynamics simulations and free energy calculations. The study identifies the roles of the active site residues and the Mg^{2+} ions in catalyzing the reaction. Of great significance, we are able to compare the free energy barrier for the reaction with that for the Mg^{2+}-assisted release of the product (i.e., pyrophosphate) into the solution, shedding light on the general mechanistic and kinetic aspects of catalysis by SNTs.

SIGNIFICANCE Sugar nucleotidyl transferases catalyze the synthesis of sugar nucleotides—essential precursors for cell wall components, bacterial antigens, and antibiotic synthesis. These enzymes employ two Mg^{2+} ions for the nucleotidyl transfer reaction. Previous studies have revealed that Mg^{2+} ions participate in the reaction as well as the product release. However, the precise role of individual Mg^{2+} ions and their influence on the kinetics of nucleotidyl transfer reaction remains to be established. Using hybrid quantum mechanics-molecular mechanics molecular dynamics simulations, we delineate the roles of Mg^{2+} ions in the reaction and identify that the Mg^{2+}-facilitated product release, rather than the chemical reaction, would control the enzymatic turnover in sugar nucleotidyltransferases.

INTRODUCTION

The enzymes belonging to the sugar nucleotidyl transferase (SNT) family catalyze nucleotidyltransfer reactions using sugar phosphate and nucleotide as their substrates, resulting in the synthesis of sugar-nucleotide and pyrophosphate. Sugar-nucleotides are the precursors for biosynthesis of cell wall components and antigens, and they participate in sugar metabolism (1–3). Several SNTs essential for bacterial survival are attractive targets for the development of new antibiotics (4–7). Besides, SNTs are considered to be potential biocatalysts for the production of glycosylated pharmaceuticals, in which sugar-nucleotides are used as the precursors (8–12). Experimental studies on these enzymes have identified catalytically crucial residues and established that Mg^{2+} ions are essential for their enzymatic activity (12–14). However, none of these studies have precisely discerned the catalytic mechanism of this enzymatic reaction.

Here, we present the mechanism of nucleotidyltransfer reaction in GlmU, which belongs to the family of SNT enzymes. Structural and biochemical studies on GlmU and other SNTs have unanimously identified that the conserved active site residues—arginine (Arg19 in GlmU) and lysine (Lys26 in GlmU)—are crucial for the nucleotidyltransfer reaction (Fig. 1 *a*; (7,12–18)). These studies proposed that Arg19 orients the nucleotide substrate in a catalytically competent conformation. It is also believed to be important for the orientation of the negatively charged substrates (UTP and GlcNAc-1-P) at the active site for the nucleotidyltransfer reaction (7,18). The side chain of Lys26 has been proposed to stabilize the leaving group of the nucleotide substrate (7,18). Moreover, experimental studies have established that Mg^{2+} ions are essential for catalysis in SNTs (12–14). A crystal structure of GlmU bound to both the productsUDP-GlcNAc (termed as UD1 from hereon) and pyrophosphate (hereafter termed as POP) and two Mg^{2+} ions (Mg^{2+}_A and Mg^{2+}_B) revealed that the enzyme recruits

Submitted February 10, 2020, and accepted for publication June 17, 2020.
*Correspondence: balaji.prakash@cftri.res.in or nnair@iitk.ac.in
Editor: Yuji Sugita.
https://doi.org/10.1016/j.bpj.2020.06.017

two Mg^{2+} ions at the active site (Fig. 1 *a*; (15,16)). This structure of GlmU identified the coordination interactions of Mg^{2+}_A and Mg^{2+}_B with the products and the active site residues (Fig. 1 *a*). Based on these interactions, it was proposed that Mg^{2+} ions would aid in catalyzing the reaction by orienting the substrates at the active site and stabilizing the transition state during nucleotidyltransfer (Fig. 1 *b*; (16)). Experimental studies on other SNTs have also proposed similar roles for the Mg^{2+} ions in catalysis (15,19). Interestingly, a subgroup of SNTs employs only a single Mg^{2+} ion (Mg^{2+}_B) (16,17). In these SNTs, Mg^{2+}_A is replaced by the positively charged side chain: the NH_3^+ group of an active site lysine (Lys421) (Fig. S1; (16)). Overall, the general mechanistic picture provided by the experimental studies on GlmU and related SNTs is as follows. The positively charged residues, Arg19 and Lys26, and the active site Mg^{2+} ion(s) (Mg^{2+}_A/Lys421 and Mg^{2+}_B) would stabilize and precisely orient the negatively charged substrates for the nucleotidyltransfer reaction (Fig. 1; Fig. S1). The reaction would ensue by the nucleophilic attack of the phosphate oxygen of GlcNAc-1-P (referred to as Gn1 from hereafter) on to the α-phosphate of UTP (Fig. 1 *b*).

In our previous x-ray crystallographic and computational study, we identified the role of Mg^{2+}_B in the release of product (pyrophosphate) from the active site (20). Thus, Mg^{2+}_B, conserved across all SNTs, is recognized to participate in both the enzymatic reaction and the subsequent product release (15–17,20). The free energy barrier for the dissociation of pyrophosphate-Mg^{2+}_B complex from the active site was computed to be 18 kcal mol^{-1}. (20) Such a high free energy barrier suggested that the process of pyrophosphate-Mg^{2+}_B release, rather than nucleotidyltransfer reaction, could be the slowest step in the catalytic cycle of GlmU and other SNTs.

In summary, this work addresses the following questions that remain unanswered: 1) mechanism and free energetics of the nucleotidyltransfer reaction, 2) role of conserved Mg^{2+}_B ion and other active site residues in the reaction, and 3) comparison of free energies for the nucleotidyltransfer reaction and product release.

We employ computational methods to investigate these aspects. Both hybrid quantum mechanics-molecular mechanics (QM/MM) (21,22) and MM (23)-based molecular dynamics (MD) simulations were performed. Metadynamics (24) simulations were carried out to obtain the mechanism and to compute the free energy barriers of the nucleotidyltransfer reaction. Although there is no dispute over the general mechanism proposed for this reaction in SNTs, to our best knowledge, this is the first theoretical study that reports the reaction mechanism and free energetics of these reactions in SNTs. These calculations are crucial for making predictions on the overall kinetics of the catalytic reactions and on the nature of catalysis in the nucleotidyltransferase domain of SNTs, in particular GlmU.

METHODS

System setup and MM MD simulations

Precatalytic structure of GlmU was obtained from the crystal structure of the GlmU-product complex bound to Mg^{2+}_A and Mg^{2+}_B (Protein Data Bank, PDB: 4G87), by replacing the products (UD1 and POP) with the substrates (UTP and GlcNAc-1-P) at the active site, for simulating uridyltransfer reaction (16). GlmU is a bifunctional enzyme with uridyltransferase activity at the N-terminal domain and the acetyltransferase activity at its C-terminal domain (25). Both the active sites are independent of each other (25). Therefore, in our simulations, GlmU was truncated to include only the N-terminal uridyltransferase domain. The first three turns from the LβH structure of the C-terminal domain were also included because they have been experimentally shown to be important for the uridyltransfer reaction (26). The LβH holds an α-helix of the N-terminal domain in a stable conformation that provides Asn239 coordinated to Mg^{2+}_A. To ensure that the α-helix of the N-terminal domain remains in a stable conformation, the LβH was held in a stable conformation by harmonic constraints throughout the simulations.

The enzyme was solvated with 14,453 TIP3P water molecules within a periodic box of dimension $70 \times 88 \times 96$ $Å^3$. The system was neutralized by adding 15 Na^+ counterions. The whole protein was treated with the parm99 version of the AMBER force field (27). Force field parameters for the ligands (UD1, POP, and two Mg^{2+} ions) were derived from the GAFF force field (28), which is compatible with the standard AMBER force field, as available in the AMBER (23) suite of programs. Missing force field parameters for the ligands were not present in the GAFF force field and were derived using Antechamber tool (29) available in the AMBER package. Restrained electrostatic potential (RESP) charges were calculated for the ligands (Gn1, UTP, and GlcNAc-1-P) and Mg^{2+} ions by the R.E.D. package (30–32). See below for details of the RESP charge calculation. Classical MD simulations were carried out using the AMBER suite of programs (23). A 12-Å cutoff distance was used while computing the nonbonded interactions. The long-range electrostatic interactions were computed using the particle mesh Ewald method (33). After the preliminary minimization of water molecules and the subsequent minimization of the whole system, NPT simulations were carried out for 1 ns at 300 K using Langevin thermostat (34) and 1 atm using Berendsen barostat. This was followed by 5-ns NVT simulation at the equilibrium volume. We used a time step of 1 fs for integrating the equations of motion.

The substrates (Gn1 & UTP), two Mg^{2+} ions (Mg^{2+}_A & Mg^{2+}_B), and truncated forms of active site residues Asp114 (acetate ion), Asn239 (acetamide), and Lys26 (methylamine) obtained from the structural model of the precatalytic form of GlmU were used for the RESP charge calculations. The total charge of the active site was restrained to $-2e$ in these calculations. Similarly, the RESP charges for the substrates in the absence of Mg^{2+}_B were calculated with the total charge of the active site restrained to $-4e$. Further details of the simulation of enzyme-substrate complex in the absence of Mg^{2+}_B are given in the Supporting Materials and Methods, Section S5.

QM/MM simulations

The coordinates of the GlmU-substrate complex after the MM equilibration simulations were taken to start the QM/MM simulations. These calculations were carried out using the CPMD/GROMOS interface program (35,36). The QM subsystem includes Gn1, UTP^{4-}, Mg^{2+}_A, Mg^{2+}_B ion, and the side chains of Arg19 and Lys21. The covalent bonds cleaved at the interface of QM and MM regions were saturated by the link hydrogen atoms. The QM subsystem was treated by plane wave density-functional theory with the Perdew-Burke-Ernzerhof exchange correlation functional (37). A plane wave cutoff of 25 Ry was taken, and ultrasoft pseudopotentials were chosen for all the QM atoms (38). The electronic embedding scheme proposed by Laio et al. (39) was employed for treating QM/MM interactions. Here, the interaction of the charge density with the point charge was considered within 15 Å of the QM electron density. The rest of the MM atoms were allowed to interact with the multipoles of the electrostatic potential because

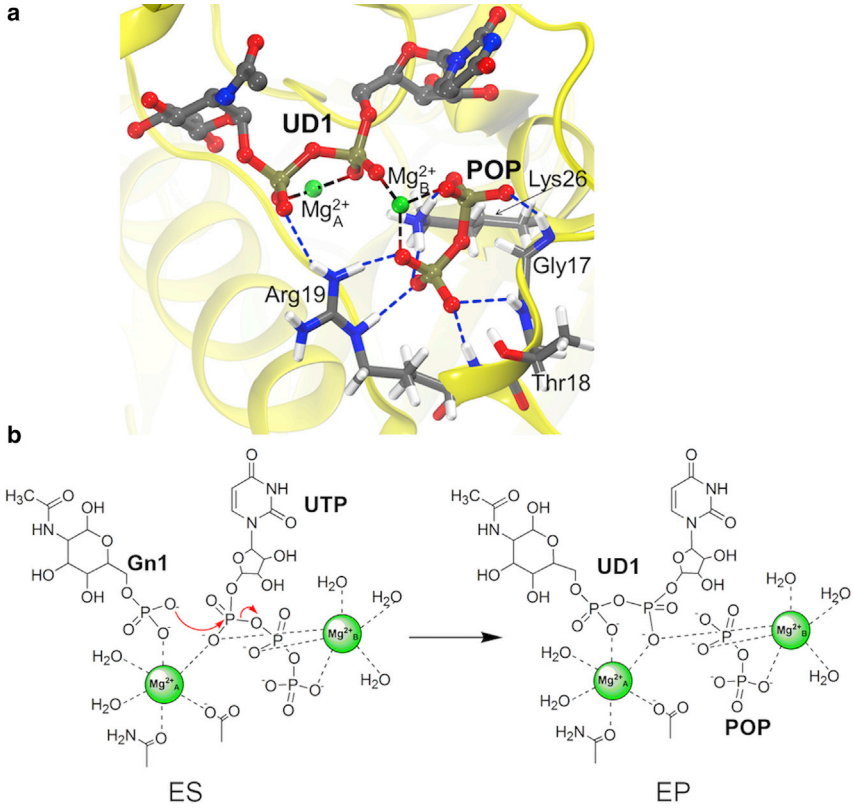

FIGURE 1 (*a*) Active site of GlmU bound to the products (UD1 and POP) and two Mg^{2+} ions (Mg^{2+}_A and Mg^{2+}_B) in the crystal structure (PDB: 4G87). UD1 (without H atoms) and POP are shown in the ball and stick model; Mg^{2+} ions are shown as green spheres. Active site residues (Gly17, Thr18, Arg19, and Lys26) are shown in the stick form. Interactions of UD1 and POP with the active site residues are shown by blue-colored dashed lines, whereas their interactions of Mg^{2+}_A and Mg^{2+}_B are denoted by black-colored dashed lines. The water molecules coordinating Mg^{2+} ions and the residues coordinating Mg^{2+}_A are not shown to enhance clarity. (*b*) Schematic diagram depicting the general mechanism proposed for the nucleotidyltransfer reaction. Arg19 and Lys26 are not shown here, to enhance clarity. To see this figure in color, go online.

of QM charge density. The MM atoms included in the QM/MM interaction exclusion list interacted with the QM atoms through dynamically generated electrostatic potential charges of the QM atoms (40). Separate Nosé-Hoover chain thermostats (41) were used for the QM and the MM systems. The Car-Parrinello MD scheme (42) was employed for the dynamics of the QM part. We chose the fictitious orbital mass as 700 a.u. The MD time step was taken as 0.145 fs. During the QM/MM equilibration of GlmU-substrate complex in the absence of Mg^{2+}_B, C_α atoms of Thr18, Arg19, and Lys26 were constrained to prevent Arg19 and Lys26 side chains from taking over the role of Mg^{2+}_B by forming stronger interactions with the α-phosphate of UTP (see Supporting Materials and Methods, Section S5 for further details). The total simulation times for QM/MM equilibration of GlmU-substrate complex in the presence and absence of Mg^{2+}_B were 20 and 14 ps, respectively.

Metadynamics simulations

Nucleotidyltransfer reaction was accelerated in the QM/MM MD simulations using the extended Lagrangian WT-MTD (43,44). Collective variables (CVs) and associated auxiliary variables were harmonically coupled, using the force constant $k_\alpha = 1.3 \times 10^3$ kcal mol^{-1}, and the fictitious mass parameter of the auxiliary variables was chosen to be 50.0 a.m.u. (Bohr)^2. The initial Gaussian height was 1.8 kcal mol^{-1} and the Gaussian width was 0.05 (unitless). For the WT-MTD, ΔT parameter was taken as 7500 K. Metadynamics bias was updated every 29 fs. The CVs used in the WT-MTD simulations are listed in Table 1.

The coordination number of atom A with a group of atoms B, CN[A:B], is defined as

$$\mathrm{CN[A:B]} = \sum_{J \epsilon \mathrm{B}} \frac{1 - \left(\frac{d[\mathrm{A}-J]}{d^0_{\mathrm{AB}}}\right)^6}{1 - \left(\frac{d[\mathrm{A}-J]}{d^0_{\mathrm{AB}}}\right)^{12}}.$$

For the values of $d[\mathrm{A}-J]$, i.e., the distance between atom A and J, less than d^0_{AB}, the fraction inside the sum approaches 1 or else it approaches to zero with the increase of $d[\mathrm{A}-J]$. The values of d^0_{AB} used in this study for various atom pairs are given in Table S1. The free energy surface $F(\mathbf{s})$ of the reaction was constructed based on the bias potential $V^b(s, t)$, as

$$F(s) = -\frac{T+\Delta T}{\Delta T} V^b(s, t \to \infty),$$

where **s** is the vector of CVs, t is the simulation time, and T is the temperature.

Convergence of free energy barrier in the MTD-1 run was monitored as a function of number of recrossings from the reactant basin to the product basin; see Table S2. Based on this data, we have taken the free energy barrier of the simulation as 8 kcal mol^{-1}.

For MTD-2 and MTD-3, the total metadynamics time was 3.1 and 4.8 ps, respectively.

TABLE 1 The CVs used for the WT-MTD simulations

Metadynamics		
MTD-1	CV1	$CN[O_{Gn1}:P_\alpha]$-$CN[P_\alpha:O_b]$
	CV2	$CN[O_b:H1_{Lys}, H2_{Lys}, H3_{Lys}]$
MTD-2	CV3	$CN[O_{Gn1}:P_\alpha]$
	CV4	$CN[P_\alpha:O_b]$
MTD-3	CV1	$CN[O_{Gn1}:P_\alpha]$-$CN[P_\alpha:O_b]$
	CV2	$CN[O_b:H1_{Lys}, H2_{Lys}, H3_{Lys}]$

The atom labels are shown in Fig. S2.

RESULTS AND DISCUSSION

Nucleotidyltransfer reaction catalyzed by GlmU: mechanism and free energetics

Nucleotidyltransfer reaction in GlmU involves the nucleophilic attack by the phosphate oxygen of Gn1 on the α-phosphate of UTP (Fig. 1 *b*). To determine the mechanism and free energy barrier of this reaction, we performed QM/MM MD simulations coupled with well-tempered-metadynamics-based enhanced sampling. This simulation, termed as MTD-1, was performed by biasing two CVs, namely CV1 and CV2 (see Fig. S2; Table 1). More details are given in the Methods and Supporting Materials and Methods Sections S2 and S3. CV1 is the difference between the coordination number (unitless) of O_{Gn1}-P_α and P_α-O_b, which was selected to sample the bond formation and the bond-breaking events during the nucleotidyltransfer reaction (Fig. S2). To also explore the possibility of proton transfer from the Lys26 side-chain amino ($-NH_3^+$) group to the leaving group oxygen (O_b), either during or succeeding the nucleotidyltransfer, we biased CV2 as well. Here, CV2 is the coordination number (unitless) of O_b and the H atoms of the Lys26 side chain $-NH_3^+$.

In MTD-1, we observed the nucleotidyltransfer reaction (**ES** → **EP**) and the backward reaction (**EP** → **ES**) multiple times. The free energy barrier for the nucleotidyltransfer reaction is 8 kcal mol^{-1}, whereas that for the reverse reaction is 22 kcal mol^{-1} (Fig. 3*a*). During the reaction, both $Mg^{2+}{}_A$ and $Mg^{2+}{}_B$ were coordinated to the oxygen atoms of the α-phosphate of UTP. Interestingly, proton transfer from the Lys26 side chain to O_b was not observed, though an H-bond interaction between Lys26 side chain $-NH_3$ and O_b (leaving group) was seen throughout the reaction (Fig. 2, *b* and *c*). Thus, the products formed after the **ES** → **EP** reaction are UD1 and deprotonated POP (Fig. 2 *c*). In both reactant and the product states, the phosphate groups make stabilizing interactions with the side chains of Arg19 and Lys26, as well as with the backbone amides of Gly17, Thr18, and Arg19 (Fig. 2, *b* and *c*). Of these residues, Arg19 and Lys26 are conserved in all SNTs (16). The Arg19 side chain makes stabilizing interactions with the phosphate of Gn1 and the γ-phosphate of UTP in the reactant state; these interactions remain intact with the phosphates of UD1 and POP in the product state (Fig. 2, *b* and *c*). The backbone amides of Gly17, Thr18, and Arg19 stabilize the β- and γ-phosphates of UTP in the reactant state. These phosphates constitute the pyrophosphate of the product and retain their interactions with the backbone amides. More detailed analysis of interactions of Gn1 and UTP with the active site is presented in Fig. S3 and Table S3. Based on these findings, we deduce that interactions between the phosphate groups and the active site residues Gly17, Thr18, Arg19, and Lys26 are potentially important for substrate stabilization and the reaction.

The role of Lys26 in the nucleotidyltransfer reaction

To further ascertain the role of Lys26, we carried out an independent metadynamics simulation MTD-2 in which two CVs were used for enhanced sampling, viz. coordination number of the O_{Gn1}-P_α (CV3) and coordination number of

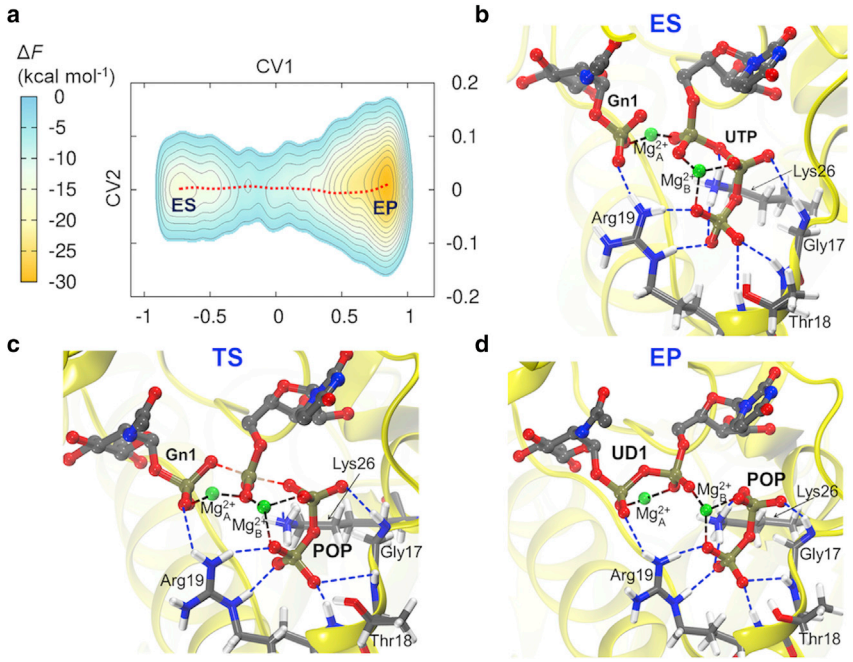

FIGURE 2 Results from MTD-1 simulation of the nucleotidyltransfer reaction in GlmU. (*a*) Reconstructed free energy surface from MTD-1; CV1 and CV2 are unitless and are defined in Table 1. The minimum free energy pathway on the computed surface is also shown (*red-dotted line*). The snapshots representing (*b*) the reactant "**ES**" state, (*c*) the likely transition state "**TS**," and (*d*) the product "**EP**" state are shown. The water molecules coordinating to Mg^{2+} ions and the residues coordinating to $Mg^{2+}{}_A$ are not shown for the purpose of clarity. Crucial distances are listed in the Table S3. To see this figure in color, go online.

the P_α-O_b (CV4) (shown by double-headed arrows in Fig. S2). It may be noted that in MTD1, we defined CV1 as the difference of CV3 and CV4. Notably, CV2 is not used in MTD-2, and therefore, we are not explicitly sampling the proton transfer between Lys26 and O_b. In MTD-2, nucleotidyltransfer reaction occurs with the free energy barrier of 18 kcal mol^{-1} (Fig. 3 *a*), which is significantly higher than that computed from MTD-1 (8 kcal mol^{-1}). Although the proton transfer from Lys26 to O_b is not observed in these metadynamics simulations, the difference in their computed energy is arising from the poor sampling of orientation of Lys26 with the phosphate group in MTD-2 simulations. This is clear from Fig. 3 *b*, in which we have plotted the distance between O_b and Lys26-N_z computed from MTD-1 and MTD-2 simulations. This signifies that orientation of Lys26 has effect on the free energetics of the nucleotidyltransfer reaction.

The role of $Mg^{2+}{}_B$ in the SNTs

Next, we performed QM/MM metadynamics simulations to directly probe the role of $Mg^{2+}{}_B$. This was done by studying the nucleotidyltransfer reaction after removing $Mg^{2+}{}_B$ from the active site. This hypothetical system was first constructed and equilibrated at the empirical MM level through equilibration simulation. This was followed by QM/MM equilibration runs. The structure of the active site was then analyzed in detail and compared with the active site structure in the presence of $Mg^{2+}{}_B$. Of great interest, the substrates Gn1 and UTP showed distinct structural changes from its native form in the presence of $Mg^{2+}{}_B$. Mainly, the attacking O atom of Gn1 (O_{Gn1}) was observed to have more dispersed spatial (probability) density in the absence of $Mg^{2+}{}_B$ than in the native form (Fig. 4, *a* and *b*). Further, the triphosphate group of UTP undergoes a substantial conformational change (Figs. 4, *a* and *b* and S3). These conformational changes resulted in an increased distance between the reacting atoms O_{Gn1} and P_α (Fig. 4 *c*).

We performed metadynamics (termed MTD-3) to examine the reaction mechanism and its kinetics in the absence of $Mg^{2+}{}_B$, employing the same set of CVs that we used in MTD-1. Despite augmenting the bias potential to 32 kcal mol^{-1}, nucleotidyltransfer did not take place (Fig. S5 *a*). This implies that the nucleotidyltransfer requires higher energy in the absence of $Mg^{2+}{}_B$. This result ascertains the importance of $Mg^{2+}{}_B$ in the catalysis. We ascribe this to the poor relative conformation realized by the substrates in the absence of $Mg^{2+}{}_B$.

In the absence of $Mg^{2+}{}_B$, the partial positive charge on P_α is reduced compared to that seen in the presence of $Mg^{2+}{}_B$ (Fig. S5 *b*). We argue that the reduced electrophilicity of P_α in the absence of $Mg^{2+}{}_B$ prohibits the bond formation between O_{Gn1} and P_α. Besides, $Mg^{2+}{}_B$ neutralizes the negative charge developing on O_α (the $Mg^{2+}{}_B$ coordinating O atom of the α-phosphate of UTP) during P_α-O_b bond breaking (Fig. S5 *c*), which would be important for transition state stabilization. Based on this, we conclude that P_α-O_b bond breaking is likely to be hampered in the absence of $Mg^{2+}{}_B$. Overall, $Mg^{2+}{}_B$ plays crucial role in the catalysis by orienting the reacting atoms, stabilizing the transition state, and enhancing the electrophilicity of the reacting P_α.

Comparison with experimental findings

Overall, the mechanistic findings obtained from our metadynamics simulation agree well with experimental studies. Experimental studies have proposed Arg19 and Lys26 to be important for the substrate stabilization and the reaction (7,12–18). Our simulations validate the role of these residues, including Gly17 and Thr18, in stabilization of phosphate groups and the nucleotidyltransfer. The mutation of Lys26 was experimentally shown to reduce the enzymatic activity in GlmU (18). Our metadynamics simulations also bring out an important role for Lys26 in the reaction. Previous experimental studies have established that Mg^{2+} ions are essential for the enzymatic activity of SNTs. The SNTs employing single Mg^{2+} ion ($Mg^{2+}{}_B$) show negligible nucleotidyltransfer activity, which is restored upon addition of $MgCl_2$ (17). Our results also demonstrate that $Mg^{2+}{}_B$ is essential for substrate orientation and catalysis. Finally, the structure of the product (**EP**) state obtained from our metadynamics simulation resembles well with the crystal structure of GlmU-product complex (PDB: 4G87) (20) (See Fig. S7).

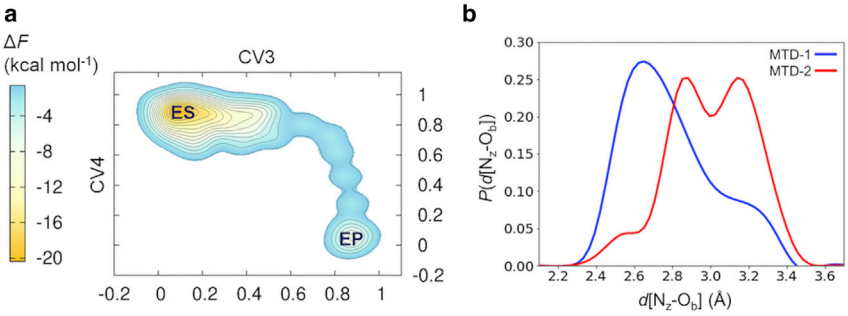

FIGURE 3 (*a*) Reconstructed free energy surface from MTD-2; CV3 and CV4 are unitless and are defined in Table 1. (*b*) Probability distribution of the distance between O_b and Lys26-N_z ($d[N_z\text{-}O_b]$) obtained from MTD-1 (*blue line*) and MTD-2 (*red line*) is plotted. To see this figure in color, go online.

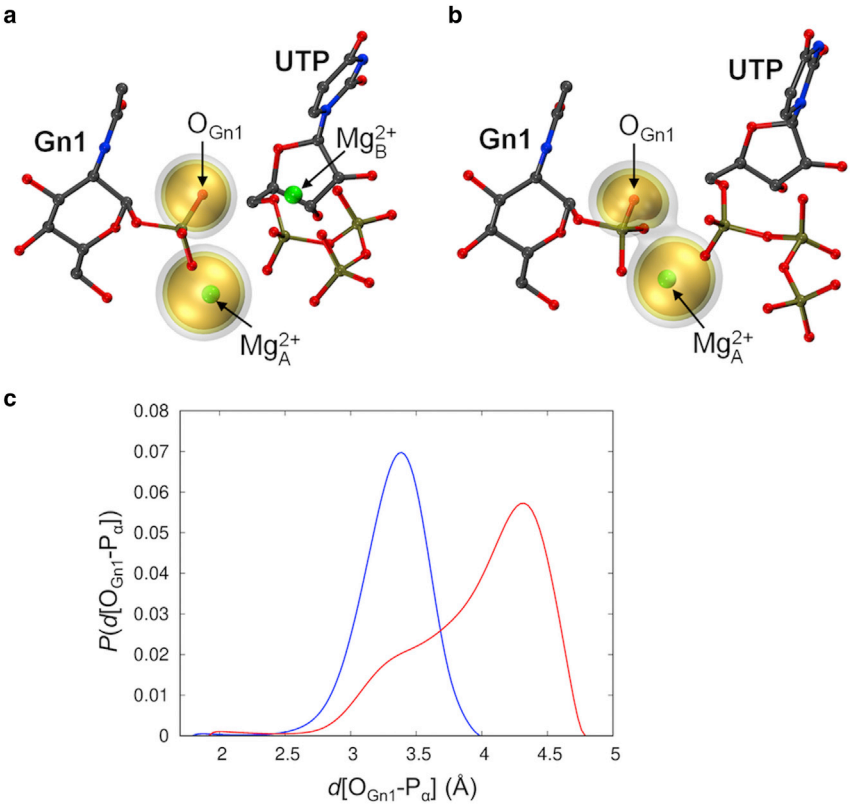

FIGURE 4 (*a* and *b*) Spatial probability distributions of the attacking oxygen atom of Gn1 (O_{Gn1}) and $Mg^{2+}{}_A$ during canonical ensemble QM/MM simulation of GlmU-substrate complex bound to (*a*) both $Mg^{2+}{}_A$ and $Mg^{2+}{}_B$ and (*b*) $Mg^{2+}{}_A$ alone (lacking $Mg^{2+}{}_B$). The isosurfaces are shown at three values: 0.25 (*white*), 0.5 (*light yellow*), and 0.75 (*golden yellow*) $Å^{-3}$. Substrates and Mg^{2+} ions are shown in ball & sticks. (*c*) Probability distributions ($Å^{-1}$) of the distance between O_{Gn1} and P_α in the presence and absence of $Mg^{2+}{}_B$ are shown in a blue and red color, respectively. To see this figure in color, go online.

The rate-determining step in the reaction ES → EP → E′ + P

We now analyze the overall free energetics of the reaction **ES → EP → E′ + P.** For this purpose, we combine the results of this study with that reported in our earlier investigation on the product release step **EP → E′ + P**. The free energy barrier for the nucleotidyltransfer elementary step (**ES → EP**) is 8 kcal mol^{-1}, and the reverse step (**EP → ES**) is 23 kcal mol^{-1}. It was found that $Mg^{2+}{}_B$ is bound to POP while it is exiting from the active site, and the free energy barrier associated with this process (**EP → E′ + P**) is 18 kcal mol^{-1}. Such a high free energy barrier for the product release was ascribed to the concomitant conformational changes of Arg19 side chain (20). The free energy barrier for the product release step is significantly higher than that of the preceding nucleotidyltransfer reaction, although the latter involves covalent bond breaking and formation (Fig. 5). However, the rate-limiting step in the reaction **ES → EP → E′ + P** is **ES → EP**. We note in passing that the relative stability of the **EP** state could also influence the turnover (as "turnover-determining intermediate") (45,46), which will be investigated in the future considering the free energetics of other elementary steps involving the catalytic cycle.

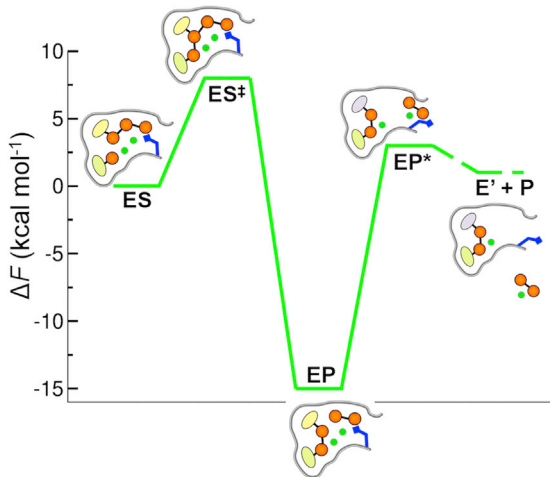

FIGURE 5 The free energy profile for the nucleotidyltransfer reaction and the POP-$Mg^{2+}{}_B$ release in GlmU. **ES**, **ES‡**, and **EP** denote the enzyme-substrate, enzyme-transition state, and enzyme-product complex, respectively, for the nucleotidyltransfer reaction. The transition state of the POP-$Mg^{2+}{}_B$ release is denoted as **EP***. Here, **E′ + P** represents the state in which the POP-$Mg^{2+}{}_B$ is released into the bulk solvent, whereas UD1 is bound at the active site. In the cartoon representation, orange spheres denote the phosphate groups and the green spheres are the Mg^{2+} ions. Arg19, which flips its conformation during the POP-$Mg^{2+}{}_B$ release, is shown as a blue-colored (*square-headed*) stick. To see this figure in color, go online.

Importance of this work in understanding the catalytic mechanism in SNTs

This study reveals several crucial protein-substrate interactions that are key to the catalytic action of GlmU. The active site residues Gly17, Thr18, Arg19, and Lys26 provide stabilizing interactions to the triphosphate group of UTP in GlmU. The same residues also stabilize POP formed after the nucleotidyltransfer reaction (Fig. 1). Backbone amides of Gly17, Thr18, and Arg19 make H-bond interactions, whereas the positively charged side chains of Arg19 and Lys26 potentially provide electrostatic stabilization. POP/triphosphate is also stabilized by Mg^{2+}_B by the coordination interactions. Mg^{2+}_B and the residues Gly17, Thr18, Arg19, and Lys26 are conserved in SNTs. The active site residues, Arg19 and Lys26, participating in the nucleotidyltransfer reaction and POP-Mg^{2+}_B release are conserved across SNTs (Fig. 6). Therefore, our findings about the critical interactions would be applicable to other SNTs too.

We find that the product release has a much higher energy barrier compared to the nucleotidyltransfer step; however, the latter is the rate-determining step while going from **ES** → **EP** → **E′** + **P.** Experimental kinetic studies on a few other class of enzymes have also identified the rate of product release to be slower than the rate of the chemical reaction in those enzymes (47–50). This is in line with our study, which shows that the POP bound to Mg^{2+}_B ion is stabilized at the active site and its release is a considerably slow process compared to the chemical reaction in GlmU. Similarly, the experimental and computational studies on a kinase identified that a catalytically important Mg^{2+} ion stabilizes the product at the active site and impedes its release from the active site (50).

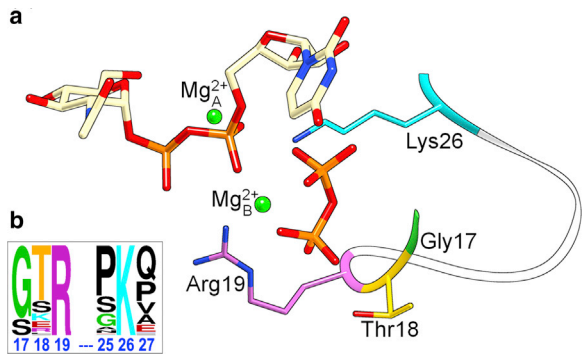

FIGURE 6 (*a*) The products UDP-GlcNAc and POP stabilized at the active site of GlmU (PDB: 4G87). Mg^{2+}_A and Mg^{2+}_B are denoted by green colored spheres. The loop providing the residues stabilizing POP is represented in the ribbon form. Gly17 (*green*), Thr18 (*yellow*), Arg19 (*magenta*), and Lys26 (*cyan*) are the residues stabilizing POP. (*b*) The conservation of POP-stabilizing residues in SNTs is represented by WebLogo frequency plot. Each stack in this logo provides information about the occurrence of amino acids at the given position. Height of the amino acid symbol denotes its relative frequency at that position. The position of residue is numbered as per the amino acid sequence (17–27) in GlmU. The amino acid symbols G (Gly), R (Arg), T (Thr), and K (Lys) are shown in green, magenta, yellow, and cyan, respectively. To see this figure in color, go online.

CONCLUSIONS

This study on the mechanism and energetics of the nucleotidyltransfer reaction catalyzed by GlmU demonstrates several features of the catalytic reaction in SNTs in general. The two Mg^{2+} ions (Mg^{2+}_A and Mg^{2+}_B) recruited by SNTs play a crucial role in nucleotidyltransfer reactions. Mg^{2+}_B orients the substrates for the reaction, stabilizes the transition state, and subsequently participates in product (POP) release. The interaction of Lys26 with the leaving phosphate group of UTP has a vital function to play in the reaction, and their relative orientation affects the free energetics of the reaction. The other conserved residues Gly17, Thr18, and Arg19 also show stable interactions with the substrate during the nucleotidyltransfer reaction. Although the free energy barrier for the nucleotidyl transferase reaction is substantially lower than that of the POP-Mg^{2+}_B release, our study reveals that the elementary step that controls the rate of the reaction **ES** → **EP** → **E′** + **P** in SNTs is the nucleotidyl transferase reaction.

SUPPORTING MATERIAL

Supporting Material can be found online at https://doi.org/10.1016/j.bpj.2020.06.017.

AUTHOR CONTRIBUTIONS

N.V., N.N.N., and B.P. designed the research. N.V. performed the research. N.V. and N.N.N. analyzed the data. N.V., N.N.N., and B.P. wrote the manuscript.

ACKNOWLEDGMENTS

QM/MM & MM simulations were performed using the High Performance Computing facility at Indian Institute of Technology Kanpur. B.P. thanks Department of Biotechnology, India, for the current grant (BT/PR12233/BRB/10/1349/2014).

REFERENCES

1. Frey, P. A. 1996. The Leloir pathway: a mechanistic imperative for three enzymes to change the stereochemical configuration of a single carbon in galactose. *FASEB J.* 10:461–470.
2. McNeil, M., M. Daffe, and P. J. Brennan. 1990. Evidence for the nature of the link between the arabinogalactan and peptidoglycan of mycobacterial cell walls. *J. Biol. Chem.* 265:18200–18206.
3. Chang, H. Y., J. H. Lee, …, H. L. Peng. 1996. Virulence and outer membrane properties of a galU mutant of *Klebsiella pneumoniae* CG43. *Microb. Pathog.* 20:255–261.
4. Mehra, R., C. Rani, …, A. Nargotra. 2016. Computationally guided identification of novel *Mycobacterium tuberculosis* GlmU inhibitory leads, their optimization, and in vitro validation. *ACS Comb. Sci.* 18:100–116.

5. Zhang, W., V. C. Jones, …, Y. Ma. 2008. Expression, essentiality, and a microtiter plate assay for mycobacterial GlmU, the bifunctional glucosamine-1-phosphate acetyltransferase and N-acetylglucosamine-1-phosphate uridyltransferase. *Int. J. Biochem. Cell Biol.* 40:2560–2571.
6. Renner-Schneck, M., I. Hinderberger, …, T. Stehle. 2015. Crystal structure of the N-acetylmuramic acid α-1-phosphate (MurNAc-α1-P) uridylyltransferase MurU, a minimal sugar nucleotidyltransferase and potential drug target enzyme in Gram-negative pathogens. *J. Biol. Chem.* 290:10804–10813.
7. Blankenfeldt, W., M. Asuncion, …, J. H. Naismith. 2000. The structural basis of the catalytic mechanism and regulation of glucose-1-phosphate thymidylyltransferase (RmlA). *EMBO J.* 19:6652–6663.
8. Gantt, R. W., P. Peltier-Pain, and J. S. Thorson. 2011. Enzymatic methods for glyco(diversification/randomization) of drugs and small molecules. *Nat. Prod. Rep.* 28:1811–1853.
9. Thibodeaux, C. J., C. E. Melançon, III, and H. W. Liu. 2008. Natural-product sugar biosynthesis and enzymatic glycodiversification. *Angew. Chem. Int.Engl.* 47:9814–9859.
10. Li, L., Y. Liu, …, P. G. Wang. 2013. Efficient enzymatic synthesis of guanosine 5′-diphosphate-sugars and derivatives. *Org. Lett.* 15:5528–5530.
11. Mizanur, R. M., and N. L. B. Pohl. 2009. Phosphomannose isomerase/GDP-mannose pyrophosphorylase from Pyrococcus furiosus: a thermostable biocatalyst for the synthesis of guanidinediphosphate-activated and mannose-containing sugar nucleotides. *Org. Biomol. Chem.* 7:2135–2139.
12. Mizanur, R. M., C. J. Zea, and N. L. Pohl. 2004. Unusually broad substrate tolerance of a heat-stable archaeal sugar nucleotidyltransferase for the synthesis of sugar nucleotides. *J. Am. Chem. Soc.* 126:15993–15998.
13. Yang, T., M. Echols, …, M. Bar-Peled. 2010. Identification and characterization of a strict and a promiscuous N-acetylglucosamine-1-P uridylyltransferase in Arabidopsis. *Biochem. J.* 430:275–284.
14. Zhou, Y., Y. Xin, …, Y. Ma. 2011. Kinetic properties of *Mycobacterium tuberculosis* bifunctional GlmU. *Arch. Microbiol.* 193:751–757.
15. Schmidt, H., J. R. Mesters, …, U. Mamat. 2011. Evidence for a two-metal-ion mechanism in the cytidyltransferase KdsB, an enzyme involved in lipopolysaccharide biosynthesis. *PLoS One.* 6:e23231.
16. Jagtap, P. K. A., S. K. Verma, …, B. Prakash. 2013. Crystal structures identify an atypical two-metal-ion mechanism for uridyltransfer in GlmU: its significance to sugar nucleotidyl transferases. *J. Mol. Biol.* 425:1745–1759.
17. Maruyama, D., Y. Nishitani, …, K. Miki. 2007. Crystal structure of uridine-diphospho-N-acetylglucosamine pyrophosphorylase from Candida albicans and catalytic reaction mechanism. *J. Biol. Chem.* 282:17221–17230.
18. Brown, K., F. Pompeo, …, Y. Bourne. 1999. Crystal structure of the bifunctional N-acetylglucosamine 1-phosphate uridyltransferase from *Escherichia coli*: a paradigm for the related pyrophosphorylase superfamily. *EMBO J.* 18:4096–4107.
19. Sivaraman, J., V. Sauvé, …, M. Cygler. 2002. Crystal structure of *Escherichia coli* glucose-1-phosphate thymidylyltransferase (RffH) complexed with dTTP and Mg2+. *J. Biol. Chem.* 277:44214–44219.
20. Vithani, N., P. K. Ankush Jagtap, …, B. Prakash. 2018. Mechanism of Mg^{2+}-accompanied product release in sugar nucleotidyltransferases. *Structure.* 26:459–466.e3.
21. Warshel, A., and M. Levitt. 1976. Theoretical studies of enzymic reactions: dielectric, electrostatic and steric stabilization of the carbonium ion in the reaction of lysozyme. *J. Mol. Biol.* 103:227–249.
22. Brunk, E., and U. Rothlisberger. 2015. Mixed quantum mechanical/molecular mechanical molecular dynamics simulations of biological systems in ground and electronically excited states. *Chem. Rev.* 115:6217–6263.
23. Pearlman, D. A., D. A. Case, …, P. Kollman. 1995. AMBER, a package of computer programs for applying molecular mechanics, normal mode analysis, molecular dynamics and free energy calculations to simulate the structural and energetic properties of molecules. *Comput. Phys. Commun.* 91:1–41.
24. Laio, A., and M. Parrinello. 2002. Escaping free-energy minima. *Proc. Natl. Acad. Sci. USA.* 99:12562–12566.
25. Mengin-Lecreulx, D., and J. van Heijenoort. 1994. Copurification of glucosamine-1-phosphate acetyltransferase and N-acetylglucosamine-1-phosphate uridyltransferase activities of Escherichia coli: characterization of the GlmU gene product as a bifunctional enzyme catalyzing two subsequent steps in the pathway for UDP-N-acetylglucosamine synthesis. *J. Bacteriol.* 176:5788–5795.
26. Parikh, A., S. K. Verma, …, V. K. Nandicoori. 2009. PknB-mediated phosphorylation of a novel substrate, N-acetylglucosamine-1-phosphate uridyltransferase, modulates its acetyltransferase activity. *J. Mol. Biol.* 386:451–464.
27. Cheatham, T. E., III, P. Cieplak, and P. A. Kollman. 1999. A modified version of the Cornell et al. force field with improved sugar pucker phases and helical repeat. *J. Biomol. Struct. Dyn.* 16:845–862.
28. Wang, J., R. M. Wolf, …, D. A. Case. 2004. Development and testing of a general amber force field. *J. Comput. Chem.* 25:1157–1174.
29. Wang, J., W. Wang, …, D. A. Case. 2006. Automatic atom type and bond type perception in molecular mechanical calculations. *J. Mol. Graph. Model.* 25:247–260.
30. Dupradeau, F.-Y., A. Pigache, …, P. Cieplak. 2010. The R.E.D. tools: advances in RESP and ESP charge derivation and force field library building. *Phys. Chem. Chem. Phys.* 12:7821–7839.
31. Vanquelef, E., S. Simon, …, F. Y. Dupradeau. 2011. R.E.D. Server: a web service for deriving RESP and ESP charges and building force field libraries for new molecules and molecular fragments. *Nucleic Acids Res.* 39:W511–W517.
32. Bayly, C. I., P. Cieplak, …, P. A. Kollman. 1993. A well-behaved electrostatic potential based method using charge restraints for deriving atomic charges: the RESP model. *J. Phys. Chem.* 97:10269–10280.
33. Darden, T., D. York, and L. Pedersen. 1993. Particle mesh Ewald: an $N \cdot \log(N)$ method for Ewald sums in large systems. *J. Chem. Phys.* 98:10089–10092.
34. Loncharich, R. J., B. R. Brooks, and R. W. Pastor. 1992. Langevin dynamics of peptides: the frictional dependence of isomerization rates of N-acetylalanyl-N'-methylamide. *Biopolymers.* 32:523–535.
35. Marx, D., and J. Hutter. 2000. Ab Initio Molecular Dynamics: Theory and Implementation. Cambridge University Press, Cambridge, UK.
36. Andreoni, W., and A. Curioni. 2000. New advances in chemistry and materials science with CPMD and parallel computing. *Parallel Comput.* 26:819–842.
37. Perdew, J. P., J. A. Chevary, …, C. Fiolhais. 1992. Atoms, molecules, solids, and surfaces: applications of the generalized gradient approximation for exchange and correlation. *Phys. Rev. B Condens. Matter.* 46:6671–6687.
38. Vanderbilt, D. 1990. Soft self-consistent pseudopotentials in a generalized eigenvalue formalism. *Phys. Rev. B Condens. Matter.* 41:7892–7895.
39. Laio, A., J. VandeVondele, and U. Rothlisberger. 2002. A Hamiltonian electrostatic coupling scheme for hybrid Car-Parrinello molecular dynamics simulations. *J. Chem. Phys.* 116:6941–6947.
40. Laio, A., J. VandeVondele, and U. Rothlisberger. 2002. D-RESP: dynamically generated electrostatic potential derived charges from quantum mechanics/molecular mechanics simulations. *J. Phys. Chem. B.* 106:7300–7307.
41. Martyna, G. J., M. L. Klein, and M. Tuckerman. 1992. Nosé–Hoover chains: the canonical ensemble via continuous dynamics. *J. Chem. Phys.* 97:2635–2643.
42. Car, R., and M. Parrinello. 1985. Unified approach for molecular dynamics and density-functional theory. *Phys. Rev. Lett.* 55:2471–2474.
43. Iannuzzi, M., A. Laio, and M. Parrinello. 2003. Efficient exploration of reactive potential energy surfaces using Car-Parrinello molecular dynamics. *Phys. Rev. Lett.* 90:238302–238304.
44. Barducci, A., M. Bonomi, and M. Parrinello. 2011. Metadynamics. *Wiley Interdiscip. Rev. Comput. Mol. Sci.* 1:826–843.

45. Kozuch, S. 2012. A refinement of everyday thinking: the energetic span model for kinetic assessment of catalytic cycles. *Wiley Interdiscip. Rev. Comput. Mol. Sci.* 2:795–815.

46. Kozuch, S. 2015. Steady state kinetics of any catalytic network: graph theory, the energy span model, the analogy between catalysis and electrical circuits, and the meaning of "mechanism.". *ACS Catal.* 5:5242–5255.

47. Furfine, E. S., J. J. Leban, …, P. J. Casey. 1995. Protein farnesyltransferase: kinetics of farnesyl pyrophosphate binding and product release. *Biochemistry.* 34:6857–6862.

48. Yao, L., Y. Li, …, H. Yan. 2005. Product release is rate-limiting in the activation of the prodrug 5-fluorocytosine by yeast cytosine deaminase. *Biochemistry.* 44:5940–5947.

49. Tallsjö, A., and L. A. Kirsebom. 1993. Product release is a rate-limiting step during cleavage by the catalytic RNA subunit of *Escherichia coli* RNase P. *Nucleic Acids Res.* 21:51–57.

50. Jacobsen, D. M., Z. Q. Bao, …, M. A. Young. 2012. Price to be paid for two-metal catalysis: magnesium ions that accelerate chemistry unavoidably limit product release from a protein kinase. *J. Am. Chem. Soc.* 134:15357–15370.